

Estimation of Empirical Green's Tensor Spatial Derivative Elements: A Preliminary Study Using Strong Motion Records in Southern Fukui Prefecture, Japan



Michihiro Ohori

1 Introduction

The empirical Green's tensor spatial derivative (EGTD) method, proposed by Plicka and Zahradnik (1998), has the potential to deal with differences in focal mechanisms between a targeted event and other small events, and to predict the ground motion for an event with an arbitrary focal mechanism. The EGTD elements are estimated through a form of single-station inversion using waveform data from several small events whose focal mechanisms and source time functions have been well determined. Although this technique is expected to provide results of considerable accuracy and prediction stability, discussion of its application has been limited in the literature (Ito et al. 2001; Ito 2005; Pulido et al. 2006; Ohori and Hisada 2006, 2011; Ohori 2014, 2016). Further data accumulation and investigation will enhance the applicability of the EGTD method. I estimated the EGTD using seven small events (M_J 3.7–4.2) in the southern part of Fukui Prefecture, Japan. Fukui Prefecture is an area with relatively low seismicity compared with other parts of Japan and strong motion data for EGTD estimation is less abundant. Most of the events used in this study occurred within or near the Mikata Fault Zone, where earthquakes of magnitude 7.2 are expected with a recurrence period of 3,800–6,300 years (Ishibe and Shimazaki 2012). In my recent work (Ohori 2016), I targeted 0.25–1 Hz bandpass filtered velocity waveforms obtained at FK1007, one of the K-NET stations operated by the National Research Institute for Earth Science and Disaster Prevention (NIED). In this article, I target velocity waveforms bandpass-filtered between 0.25 and 1 Hz and 0.25 and 10 Hz obtained at three stations, including FK1007. There are nuclear power stations of various types along the coastal area close to the fault.

M. Ohori (✉)

Research Institute of Nuclear Engineering, University of Fukui, 1-3-33 Kanawa, Tsuruga
914-0055, Japan
e-mail: ohorim@u-fukui.ac.jp

This preliminary study in such an area is significant in its evaluation of the value of strong motion prediction using EGTD, which demonstrates the potential for greater use of EGTD estimation.

2 Method

The estimation method of EGTD has been explained fully by Ohori and Hisada (2006, 2011). It is applicable to simulation of strong motion in a frequency range below the corner frequency. I briefly summarize the method below. Ground motion displacement $u_i(x_o, t)$ ($i = x, y, z$), excited by a double-couple point source, is theoretically expressed as the convolution of moment tensor elements $M_{pq}(x_s, \tau)$ ($p, q = x, y, z$) and Green's tensor spatial derivative elements $G_{ip,q}(x_o, t|x_s, \tau)$.

$$u_i(x_o, t) = M_{pq}(x_s, \tau) * G_{ip,q}(x_o, t|x_s, \tau) \quad (1)$$

Hereafter, I abbreviate $u_i(x_o, t)$, $M_{pq}(x_s, \tau)$, and $G_{ip,q}(x_o, t|x_s, \tau)$ as u_i , M_{pq} , and $G_{ip,q}$. Explicit expressions of M_{pq} for a double-couple point source are available in the literature (e.g. Aki and Richards (1980)). Considering symmetrical conditions ($M_{pq} = M_{qp}$) and no volume change [$M_{xx} = -(M_{yy} + M_{zz})$] of the moment tensor elements, we can rewrite Eq. (1) as

$$u_i = \sum_{j=1}^5 M_j * G_{ij} \quad (2)$$

where M_j ($j = 1, 2, \dots, 5$) is defined by $M_1 = M_{xy}$, $M_2 = M_{yy}$, $M_3 = M_{yz}$, $M_4 = M_{xz}$, $M_5 = M_{zz}$, and G_{ij} ($j = 1, 2, \dots, 5$) is defined by $G_{i1} = G_{ix,y} + G_{iy,x}$, $G_{i2} = G_{iy,y} - G_{x,x}$, $G_{i3} = G_{iy,z} + G_{iz,y}$, $G_{i4} = G_{ix,z} + G_{iz,x}$, $G_{i5} = G_{iz,z} - G_{ix,x}$. In a moment tensor inversion, u_i and G_{ij} are given and M_j are the unknowns to be solved in a least-squares sense. Conversely, in the EGTD inversion, u_i and M_j are given and G_{ij} are the unknowns to be solved. Note that the EGTD inversion is carried out for each component at each station using data from several events simultaneously, whereas the moment tensor inversion is computed for a particular event using data of all possible components at all possible stations simultaneously. It should also be emphasized that the moment tensor elements are determined by the source parameters while the Green's tensor spatial derivative elements are dependent on the underground structure of the area surrounding both the source and the station.

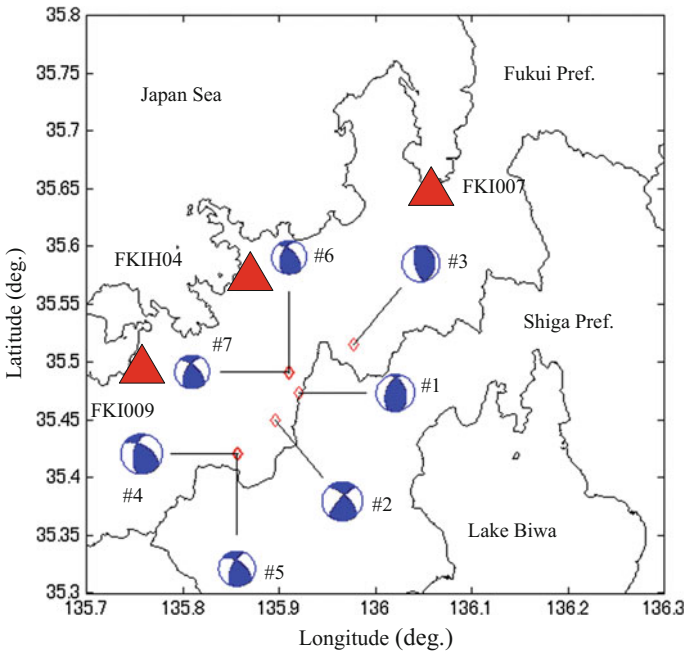


Fig. 1 Map showing epicenter locations of small events (M_j 3.7–4.2) and target stations, FKI007, FKI04, FKI009. Focal mechanisms, as determined by the F-net, are also shown. Numerals after # show correspondence to the events listed in Table 1. This figure is modified from Ohori (2016)

3 Targeted Events and Stations

Strong motion records at FKI007 and FKI009 of the K-NET stations and FKI04 of the KiK-net stations were used, all of which are operated by NIED. The map in Fig. 1 shows the stations and the epicenter locations of the target events. The source locations determined by the Japan Meteorological Agency (JMA) are summarized in Table 1. The focal mechanisms determined by the F-net (NIED) are also shown in Fig. 1. They all are classified as reverse-faulting mechanisms, but strike-slip faulting components are found in most events. Their epicentral distance was 16.1–30.8 km for FKI007, 8.2–15.3 km for FKI04, and 12.6–20.6 km for FKI009. I estimated G_{ij} , the EGTD elements of the target stations, from these small events. To treat each event as a point source at the same location with different source mechanisms, I conducted, as described below, some corrections to the focal mechanisms and the waveform data prior to EGTD estimation.

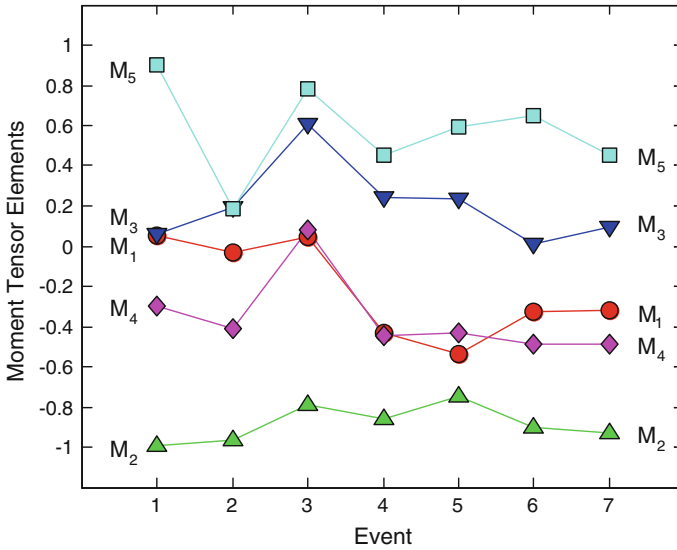


Fig. 2 Distributions of moment tensor elements of seven small events for FKI007. This figure is modified from Ohori (2016)

3.1 Correction for Focal Mechanisms

As seen in Fig. 1, the sources of the target events are almost located in a line from north-east to south-west. The station azimuth, with respect to the epicenters, is between 26.2° and 38.3° for FKI007, measured clockwise from North. It more widely varies between -63.7° and 4.5° for FKI04 and between -95.7° and -48.6° for FKI009. To compensate for this discrepancy, I selected event 2 as a reference event and horizontally rotated the focal mechanisms of the other six events so that the station azimuth of each event can be treated as the same as that of event 2. Figure 2 shows the

Table 1 The source information of target events determined by the united hypocenter catalog of the JMA (Japan Meteorological Agency)

Event	Date (y/m/d)	Clock (h:m:s)	Latitude ($^\circ$)	Longitude ($^\circ$)	Depth (km)	M _J
1	2001/04/16	19:05:18.19	35.4737	135.9208	14.30	4.0
2	2001/12/28	3:28:02.73	35.4497	135.8957	6.74	4.2
3	2003/03/13	21:04:56.02	35.5152	135.9773	14.22	4.1
4	2008/08/08	4:35:16.24	35.4213	135.8563	14.56	4.2
5	2008/08/30	18:28:30.11	35.4207	135.8573	14.51	4.2
6	2009/11/22	23:49:22.73	35.4907	135.9105	11.79	3.7
7	2009/11/22	23:52:29.04	35.7920	135.9097	11.83	3.7

distributions of moment tensor elements for seven events after the horizontal rotation with respect for FKI007. The take-off angle from each source is also different. For example, assuming the source depth as in Table 1, it varies from 100.6° to 130.3° for FKI007. In our previous study (e.g. Ohori and Hisada 2011), we examined the effect of vertical rotation of focal mechanisms to correct for differences in take-off angles and found that this is not significant when epicentral distances are larger than source depths. This seems to be effective for all source-station pairs of FKI007 and most pairs of FKI03 and FKI009. Therefore, for simplicity, I disregarded the discrepancy of the take-off angles.

3.2 Correction Applied to the Waveform Data

The observed acceleration records at three stations for seven small events were integrated into 0.25–1 Hz bandpass-filtered velocity waveform data and 0.25–10 Hz bandpass-filtered velocity waveform data. Two horizontal components were rotated into transverse and radial ones. According to Ohori (2014), corner frequencies of these small events are expected to be higher than 1 Hz, so I first targeted the frequency components lower than 1 Hz. To adjust the timing among events, I applied a time shift to the observed data to match the S-wave arrival time with that of the reference event 2. Differences in the seismic moments among events were corrected by normalization to 1.0×10^{15} Nm, approximately equal to $M_w 4.0$. To estimate the EGTD for simulation of broadband strong motion, next I targeted the 0.25–10 Hz bandpass-filtered velocity waveform data. To simulate broadband strong motion based on the empirical Green's spatial derivative method, the discrepancy among the corner frequencies of events should be removed. Ohori (2014) assumed the scaling law based on the ω^{-2} model (Aki 1967) and compensated the spectral amplitude decay beyond the corner frequency of each event so as to have the same corner frequency each other. In this study, I neglected this procedure for simplicity.

4 Results

Through the above procedure, I estimated the EGTD elements. In Fig. 3, I show example of empirical Green's tensor spatial derivative (EGTD) elements for FKI007 from bandpass-filtered velocity waveforms of 0.25–1 Hz (3a) and 0.25–10 Hz (3b). They both show very long duration characteristics in each EGTD element, after the S-wave main portion. These are difficult to produce by wave propagation theory for a stratified underground structure and reflect the complicated underground structure of the area surrounding both the source and the station. As suggested by Ohori and Hisada (2011), the EGTD elements could be useful for the structural study. In Figs. 4 and 5, I compare the observed velocity waveforms (in red) and corresponding syntheses calculated using EGTD (in blue). In Fig. 4, velocity waveform data with

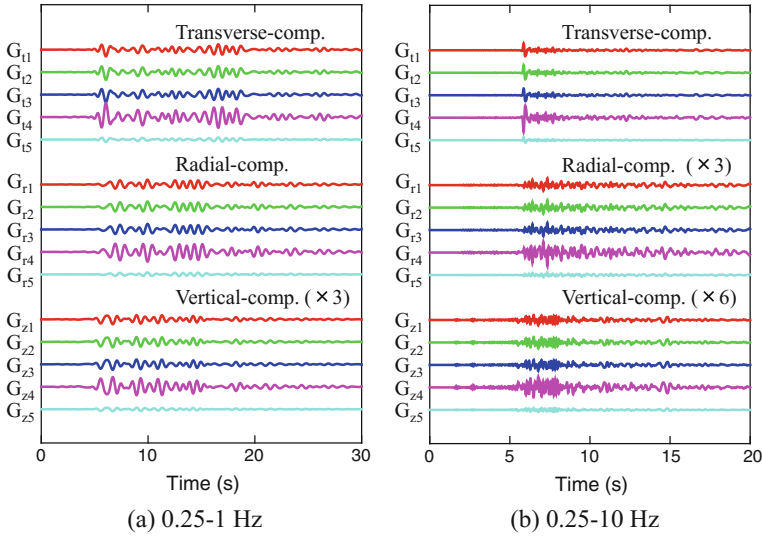


Fig. 3 Example of empirical Green's tensor spatial derivative (EGTD) elements for FK1007 estimated from 0.25–1 and 0.25–10 Hz bandpass-filtered velocity waveforms. For graphical purposes, the amplitudes of radial components in (b) and vertical components in (a) and (b) are three times or six times exaggerated compared with transverse components

0.25–1 Hz bandpass filtering are targeted. From Fig. 4, an acceptable match for the whole waveforms of all events can be found in three components, except for the underestimation found in transverse and vertical components of FKIH04 and transverse and radial components of FK1009 for event 4. In Fig. 5, velocity waveform data with 0.25–10 Hz bandpass filtering are targeted. From Fig. 5, an acceptable match for the whole waveforms of all events can be found in three components, except for the underestimation found in three components of FKIH04 and FK1009 for event 4. In Fig. 6, the ratio of the maximum amplitude between the synthesized and observed waveforms (hereafter “ratio”) are summarized. As mentioned above, except for event 4, the ratio agrees well, no more than 1.5 for most of events. To improve the underestimation for event 4 found in most cases, the slight modification of source mechanism and source time function as well as the appropriate seismic moment should be considered for this event.

5 Conclusions

I applied the EGTD method to the velocity waveforms bandpass-filtered between 0.25–1 Hz and 0.25–10 Hz, respectively. On the whole, I consider that the agreement of the simulation results obtained using the EGTD method with observation data is acceptable. To improve the waveform match, I will reconsider the appropriate source

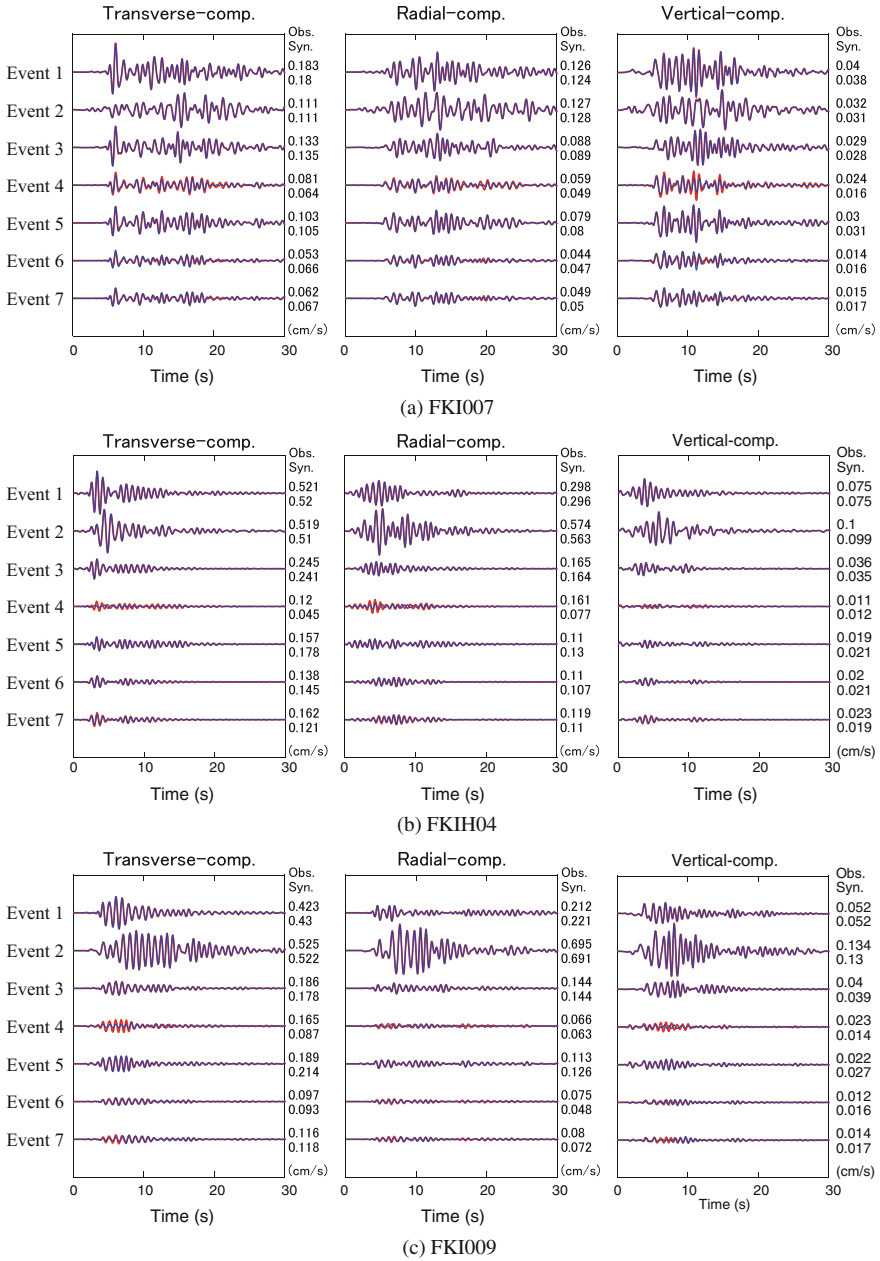


Fig. 4 Comparison of the 0.25–1 Hz bandpass-filtered observed velocity waveforms used in the EGTD estimation (in red) and the corresponding syntheses calculated from the EGTD (in blue). The absolute peak amplitude (in cm/s) is given at the end of each trace

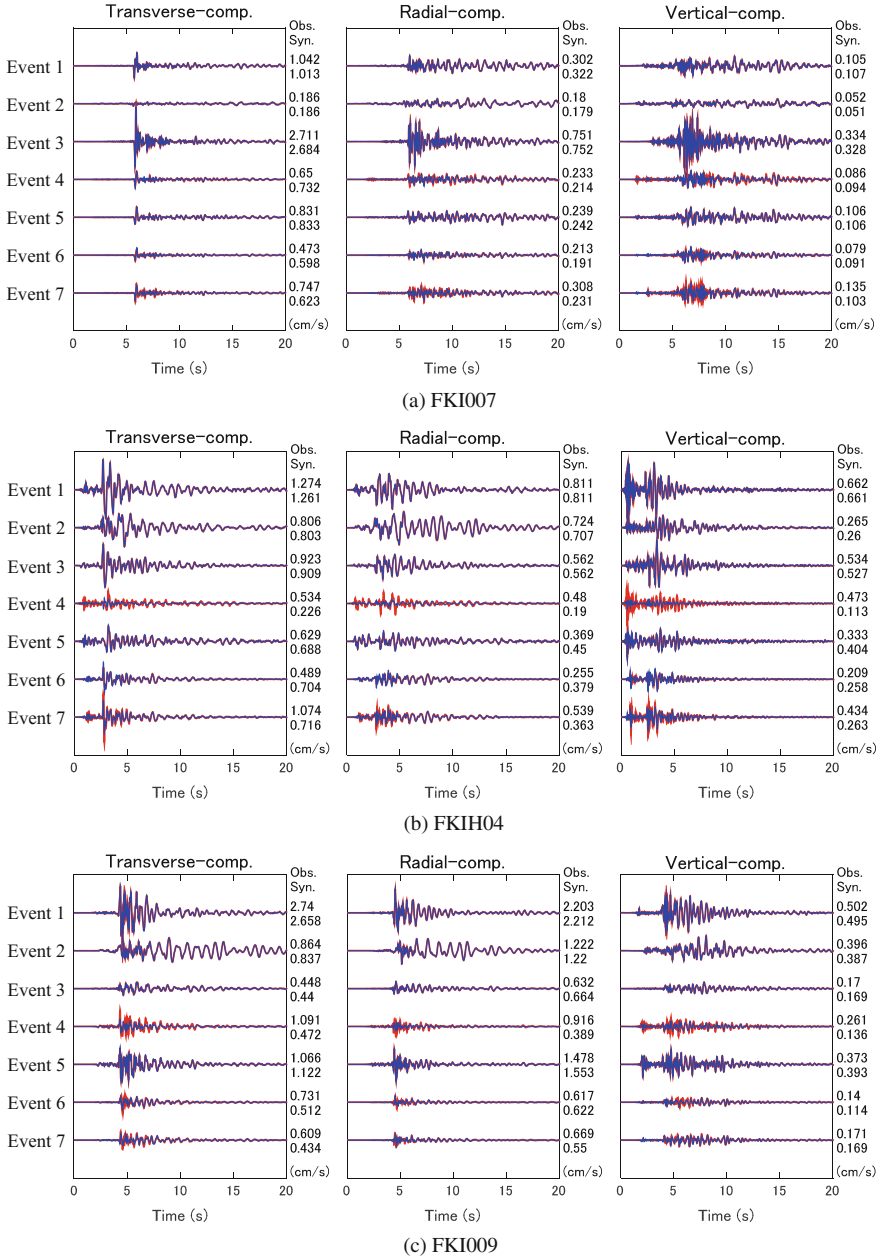


Fig. 5 Comparison of the 0.25–10 Hz bandpass-filtered observed velocity waveforms used in the EGD estimation (in red) and the corresponding syntheses calculated from the EGD (in blue). The absolute peak amplitude (in cm/s) is given at the end of each trace

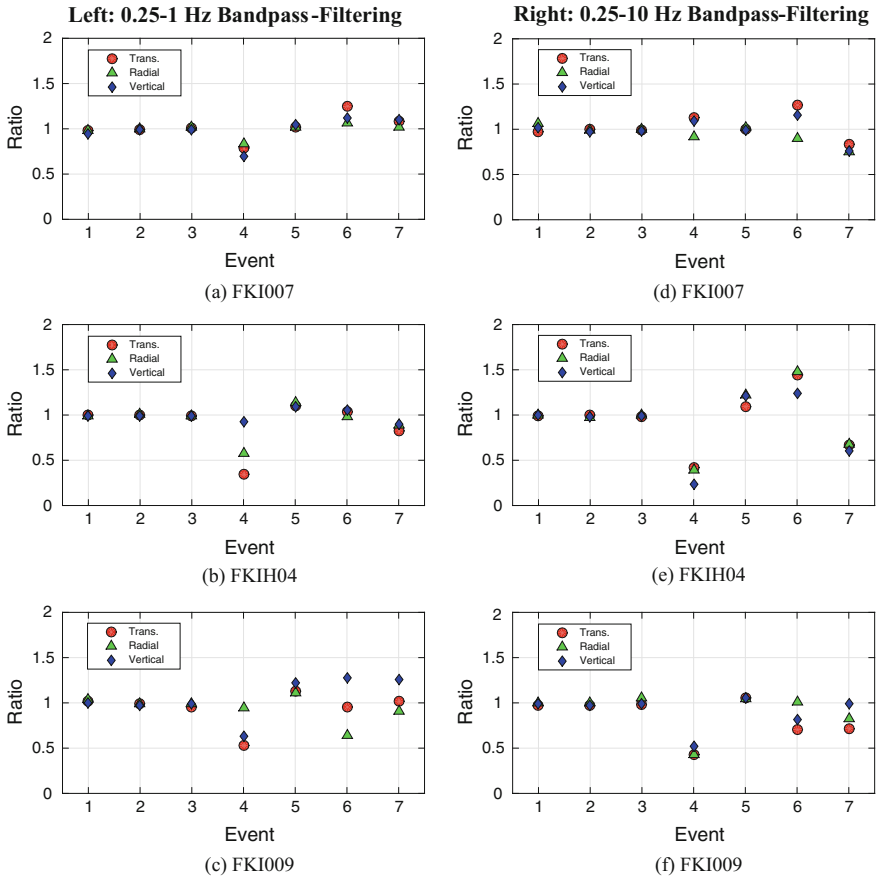


Fig. 6 Comparison of the maximum amplitude ratio between the synthesis and observatory data. Results from 0.25–1 Hz bandpass-filtered velocity waveforms are shown in (a, b, c) on a left panel, and those from 0.25–10 Hz are in (d, e, f) on a right panel

parameters (e.g. seismic moments, source mechanisms, source time functions, and corner frequencies) in a future study. The EGTD estimates in this report should be confirmed when future earthquakes occur around the same source area. I hope that this preliminary study in an area of relatively low seismicity is encouraging for the further investigation of EGTD estimation and evaluation of strong motion predictions using EGTD.

Acknowledgements The strong ground motion data used in this study were recorded at the K-NET and KiK-net stations provided by the National Research Institute for Earth Science and Disaster Prevention (NIED) on their Websites (<http://www.kyoshin.bosai.go.jp/kyoshin/>, last accessed April 2015). The Japan Meteorological Agency (JMA) unified hypocenter catalogue and the F-net source parameters were also provided by the NIED on their Website (<http://www.fnet.bosai.go.jp/freesia/>

[top.php](#), last accessed April 2015). This study was partially supported by Grants-in-Aid for Scientific Research (C) (16K01316).

References

- Aki K (1967) Scaling law of seismic spectrum. *J Geophys Res* 72(4):1217–1231
- Aki K, Richards PG (1980) *Quantitative seismology, theory and methods*. W. H. Freeman, San Francisco, p 932
- Ishibe T, Shimazaki K (2012) Characteristic earthquake model and seismicity around late quaternary active faults Japan. *Bull Seism Soc Am* 102:1041–1058
- Ito Y (2005) A study on focal mechanisms of aftershocks. Report National Res Inst Earth Sci Disaster Prev 68:27–89 (in Japanese)
- Ito Y, Okada T, Matsuzawa T, Umino N, Hasegawa A (2001) Estimation of stress tensor using aftershocks of 15 September 1998 M5.0 Sendai, NE Japan, earthquake. *Bull Earthq Res Inst* 76:51–59 (in Japanese)
- Ohori M (2014) Simulation of broadband strong motion based on the empirical Green's spatial derivative method. In: Second conference on european earthquake engineering and seismology. Istanbul, Aug 25–29
- Ohori M (2016) Estimation of empirical green's tensor spatial derivative elements: a preliminary study using strong ground motion records in southern Fukui prefecture, Japan. *J Earth Sci* 2:11–18
- Ohori M, Hisada Y (2006) Estimation of empirical green's tensor spatial derivatives using aftershocks of the 2001 Hyogo-ken Hokubu earthquake and simulation of mainshock (M_J5.4) strong motion. *Zisin (J Seismol Soc Japan)* 59:133–146. (in Japanese with English abstract)
- Ohori M, Hisada Y (2011) Comparison of the empirical Green's spatial derivative method empirical Green's function method. *Bull Seism. Soc Am* 101:2872–2886
- Plicka V, Zahradnik J (1998) Inverting seismograms of weak events for empirical Green's tensor derivatives. *Geophys J Int* 132(3):471–478
- Pulido N, Dalguer L, Fujiwara H (2006) Strong motion simulation on a dynamic fault rupture process and empirical Green's tensor derivatives. In: Fall meeting of the seismologic society of Japan, D018